Optica Applicata, Vol. XXXIX, No. 1, 2009

The serially coupled multiple ring resonator filters and Vernier effect

CHINDA CHAICHUAY[1], PREECHA P. YUPAPIN[1*], PRAJAK SAEUNG[2]

[1]Faculty of Science, King Mongkut's Institute of Technology Ladkrabang, Bangkok 10520, Thailand

[2]Department of Physics, Faculty of Science, Prince of Songkla University, Hadyai, Songkla, Thailand

[*]Corresponding author: kypreech@kmitl.ac.th

The general characteristics of serially coupled multiple ring resonator (SMRR) filters are analyzed. In this case, the ring resonators of the SMRR have identical perimeters and the coupling coefficients distribution provides passband characteristics with steeper roll-off, flatter top and greater stopband rejection than a single ring resonator. In addition, we have also designed and simulated a nonsymmetric Vernier type of SMRR filters for improving a wide free spectral range (FSR) with different ring radii. To expand the FSR of the SMRR, Vernier filters are determined by the least common multiple of the FSR of individual ring resonators. The improvement in suppression of interstitial resonances is also investigated. A novel derivation of the optical transfer functions in *Z*-domain of SMRR filters is expressed employing a graphical approach to ring resonators with unequal perimeters that can be represented in signal flow graph diagrams.

Keywords: optical filter, bandpass filter, optical ring resonator.

1. Introduction

Selective bandpass filters based on ring resonators are a key component in modern dense wavelength division multiplexing (DWDM) systems applications for the implementation of fundamental functions. The functions, such as channel add-drop, channel selection, demultiplexing and multichannel filtering are formed. Some of these functions apply to a single channel of the system, whereas others apply to a subset of channels. The required characteristics of those functions are high stopband rejection in order to guarantee a low cross-talk between channels, a flat-top filter response, and low insertion loss [1].

Since the single ring resonator (SRR) filter is insufficiently discriminating for many important applications in DWDM systems, the SMRR filters are required to achieve passbands with a shaper roll off, flatter top and higher out-off band rejection around a resonance than SRR filters described in [2, 3]. The characteristics as above--mentioned are necessary to enlarge the tolerance of wavelength error of signals and the packing efficiency of wavelength channels.

However, the SRR filter has a simple Lorentzian response. When channels are closely spaced, a Lorentzian response may not provide an adequate roll-off to minimize a cross talk between channels. Also, Lorentzian responses have a sharp peak while filter applications usually require a flat top. Therefore, the tailoring of filter response shape is required to improve the performance of ring resonator filters.

In addition, DWDM system also requires an optical channel filter whose high selectivity (namely, the ability to separate two adjacent channels) has a wide free spectral range (FSR) to accommodate large channel counts. To expand the FSR, this can be realized by using two ways as follows: one employs a ring resonator constructed using a smaller ring waveguide. The conventional SRR has a disadvantage in that it cannot increase the FSR well enough. Since FSR is proportional to the inverse of ring radius, the ring radius should be reduced in order to increase the FSR. However, bending loss of the ring waveguide increases rapidly with decreasing ring radius for FSR expansion. This is a serious problem to use optical ring resonators as tunable filters. Therefore, to avoid prohibitively large losses, either the circumference of ring resonator must be kept sufficiently large or the refractive index contrast must be high to moderate radiation loss [4]. There is, however, the other way of increasing the FSR without decreasing a ring radius. The Vernier operation, which SMRR of slightly different rings radii, is employed. This consists in expanding the FSR without reducing the ring radius but adding another ring waveguide in order to construct ring waveguide with a different FSR. Investigations on these types of filters have been reported in [5–7].

Optical filter design is typically approached with electromagnetic field equations where the fields are solved in the frequency or time domain. These techniques are required to characterize the ring resonator performances and directional couplers. However, they can become cumbersome and non-intuitive for filter design. Therefore, a different analytical method of signal processing, including the scattering matrix method [8, 9], namely, the transfer matrix/chain matrix algebraic method [8, 10, 11] has been developed for determining optical filter transfer functions in Z-domain, considering optical circuit to be linear and time invariant. The other approach to analyze the complex photonic circuit and fast calculation of optical transfer functions is a graphical approach. It is also called the signal flow graph (SFG) method proposed by MASON [12]. This method has been originally used in electrical circuits, yet has not been widely employed in the analysis of optical circuits. Altogether, this is a novel attempt to obtain the optical transfer functions of SMRR filters by using a graphical approach in the analytical derivation that can be represented in SFG diagrams, thus allowing us to apply Mason's rule to produce the equivalent photonics circuits.

2. Photonic transfer functions of ring resonators

Consider the architectures of ring-resonator add/drop filters as illustrated in Figs. 1–3, which are constructed by 2×2 optical couplers. The 2×2 optical directional coupler can be represented in a signal flow graph diagram according to [8]. By taking into account

the coupling factors κ_i of the i-th coupler ($i = 1, 2, ..., N$) and the insertion loss γ for each coupler, the light pass through the throughput path we can express as $c_i = [(1-\gamma)(1-\kappa_i)]^{1/2}$ and in contrast, the light pass through the cross path is expressed by $-js_i = -j[(1-\gamma)\kappa_i)]^{1/2}$. As to the transmission of light along the ring resonator (the close pass), we can represent it as $\xi = xz^{-1}$, where $x = \exp(-\alpha L/2)$ is the one round-trip losses coefficient, and the z^{-1} is the Z-transform parameter, which is defined as

$$z^{-1} = \exp(-j\beta L) \tag{1}$$

where $\beta = kn_{\text{eff}}$ is the propagation constant, $k = 2\pi/\lambda$ is the vacuum wave number, n_{eff} is the effective refractive index of the waveguide, and the circumference of the ring is $L = 2\pi R$, here R is the radius of the ring. When all rings of MRR have the same circumference the device is called a uniform MRR optical filters, and the FSR of the device is determined by

$$\text{FSR} = \frac{c}{n_g L} \tag{2}$$

where $n_g = n_{\text{eff}} + f_o(\mathrm{d}n_{\text{eff}}/\mathrm{d}f)_{f_o}$ is the group refractive index of the ring, n_{eff} is the effective refractive index and f_o is the design (center) frequency [8]. The optical resonators resonate at a high order mode. At the f_o, the perimeter of the ring is an integer number of guide wavelengths, and this integer M_r is the order number of the mode and $f_o = M_r$ FSR.

There are basically three essential parameters describing the behavior of a MRR filter response: *i*) the –3 dB bandwidth or the full-width at half-maximum (FWHM), *ii*) the on–off ratio, and *iii*) the shape factor. For a lossless fiber ring resonator, the –3 dB bandwidth depends mainly on the coupling coefficients and the optical round-trip length.

The on–off ratio for the throughput and drop port, which is the ratio of the on--resonance intensity to the off-resonance intensity, is given by:

$$\text{on–off ratio} = \frac{T_{\max(\text{throughput port})}}{T_{\min(\text{drop port})}} \tag{3}$$

The box-like shape of the filter response for the throughput and drop port can be described by a shape factor [7] which is defined as:

$$\text{shape factor} = \frac{-1 \text{ dB bandwidth}}{-10 \text{ dB bandwidth}} \tag{4}$$

The ideal response shape is a rectangular filter function with the shape factor of unity. High performance MRR add/drop filters can be realized using double and triple ring resonators with the specific transmission characteristic (steep roll-off, flat top and high on–off ratio >20 dB) simulated in this paper.

2.1. Mason's rule for optical circuits

A forward path is a connected sequence of directed links going from one node to another (along the link directions), encountering no node more than once. A loop is a forward path that begins and ends on the same node. The loop gain or path gain is the product of all the links along that loop or path, respectively. Two loops or paths are said to be non-touching, if they share no nodes in common. The Mason's rule states that the transfer function or input−output transmittance relationship from node $E_1(z)$ to node $E_n(z)$ in a signal flow graph is given by

$$H = \frac{1}{\Delta} \sum_{i=1}^{n} T_i \Delta_i \tag{5}$$

where H is the network function relating an input and an output port, T_i is the gain of the i-th forward path from an input to an output port, and n is the total number of forward paths from an input to an output. The signal flow graph determinant is given as

$$\Delta = 1 - \sum_{i} T_i + \sum_{i,j} T_i T_j - \sum_{i,j,k} T_i T_j T_k + \ldots \tag{6}$$

where T_i is the transmittance gain of the i-th loop. In each of the product summations, the products of non-touching loops are only included. The term "non-touching" refers to the loops that have no node in common, *i.e.*, the separated loops. The minus sign is for a sum of products of an odd number of loop gains, and the plus sign is for that of an even number of loop gains. The symbol Δ_i in (5) is the determinant Δ after all loops which touch the T_i path at any node have been eliminated. It is noted here that the optical transmittance in our paper is also used in the same graphical representation.

2.2. Transfer functions of a single ring resonator add/drop filter

The optical transfer functions of ring resonator filters at the throughput port and drop port for an input port E_1 can be obtained by using the Mason's rule. First we present the transfer function of SRR filter followed by corresponding results on double and triple ring resonator filters in Sections 2.3 and 2.4, respectively. SFG for the SRR add/drop filter is shown in Fig. 1**b**, in which the input node is $E_1(z)$ while $E_3(z)$ and $E_8(z)$ are considered as the throughput node and drop node, respectively.

2.2.1. The transfer function $\frac{E_3(z)}{E_1(z)}$

There is one individual loop gain of the SFG which is denoted as

$$L_1^1 = c_1 c_2 \xi \tag{7}$$

The forward path transmittances from node 1 to node 3 for the throughput port and its determinant which corresponds to the non-touching loop can be denoted as

$$\begin{aligned} T_{1t}^1 &= -c_2 s_1^2 \xi \\ \Delta_1 &= 1 \end{aligned} \tag{8}$$

$$T_{2t}^{1} = c_1$$
$$\Delta_2 = 1 - L_1^1 = 1 - c_1 c_2 \xi \tag{9}$$

From (6), the determinant of the SFG from the Mason's rule is given by

$$\Delta = 1 - L_1^1 = 1 - c_1 c_2 \xi \tag{10}$$

By substituting (8)–(10) into (5), the transfer function for the throughput port in Fig. 1**b** can thus be expressed as

$$\frac{E_3(z)}{E_1(z)} = H_t^1 = \frac{c_1 - c_2 \xi}{1 - c_1 c_2 \xi} \tag{11}$$

2.2.2. The transfer function $\frac{E_8(z)}{E_1(z)}$

There is only one forward path transmittance from node 1 to 8 for the drop port and this forward path also touches the loop L_1^1 given by (7); therefore we have

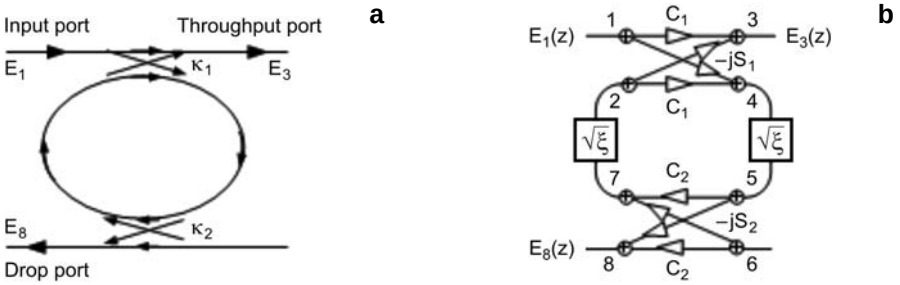

Fig. 1. The architecture of SRR add/drop filter: **a** – waveguide layout, **b** – *Z*-transform diagram (SFG).

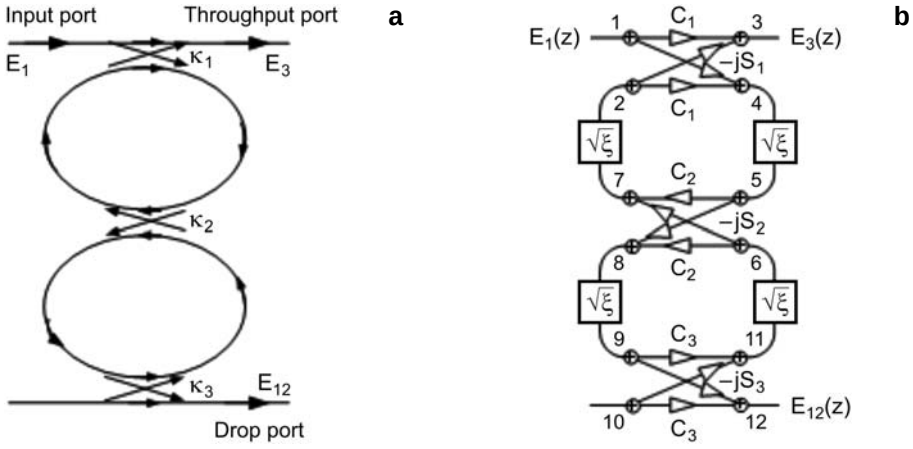

Fig. 2. The architecture of SDRR add/drop filter: **a** – waveguide layout, **b** – *Z*-transform diagram (SFG).

$$T_{1d}^{1} = -s_1 s_2 \sqrt{\xi}$$
$$\Delta_1 = 1 \tag{12}$$

Substituting (10), (12) into (5), we can obtain the transfer function for the drop port in Fig. 1**b** as

$$\frac{E_8(z)}{E_1(z)} = H_d^1 = -\frac{s_1 s_2 \sqrt{\xi}}{1 - c_1 c_2 \xi} \tag{13}$$

2.3. Transfer functions of a double ring resonator add/drop filter

SFG of a serially coupled double ring resonator (SDRR) filter is shown in Fig. 2**b**. Here the input node is $E_1(z)$ while $E_3(z)$ is considered as the throughput node and $E_{12}(z)$ is the drop node.

2.3.1. The transfer function $\frac{E_3(z)}{E_1(z)}$

There are three individual loop gains of the SFG, and all the loop gains are expressed as

$$L_1^2 = c_1 c_2 \xi \tag{14}$$

$$L_2^2 = c_2 c_3 \xi \tag{15}$$

$$L_3^2 = c_1 \sqrt{\xi}\,(-j s_2)\sqrt{\xi}\, c_3 \sqrt{\xi}\,(-j s_2)\sqrt{\xi} = c_1 c_3 s_2^2 \xi^2 \tag{16}$$

There is one possible product of transmittance of two non-touching loops, resulting from the separation of the loops L_1^2 and L_2^2, given by

$$L_{12}^2 = c_1 c_2^2 c_3 \xi^2 \tag{17}$$

The forward path transmittances from node 1 to node 3 for the throughput port and its determinant which corresponds to the non-touching loop can be denoted as

$$T_{1t}^2 = -c_2 s_1^2 \xi$$
$$\Delta_1 = 1 - L_2^2 = 1 - c_2 c_3 \xi \tag{18}$$

$$T_{2t}^2 = c_3 s_1^2 s_2^2 \xi^2$$
$$\Delta_2 = 1 \tag{19}$$

$$T_{3t}^2 = c_1$$
$$\Delta_3 = 1 - (L_1^2 + L_2^2 + L_3^2) + L_{12}^2 =$$
$$= 1 - c_1 c_2 \xi - c_2 c_3 \xi + c_1 c_3 s_2^2 \xi^2 + c_1 c_2^2 c_3 \xi^2 \tag{20}$$

From (6) and by using the relation $s_2^2 + c_2^2 = 1$, the determinant of the SFG from the Mason's rule is given by

$$\Delta = 1 - (L_1^2 + L_2^2 + L_3^2) + L_{12}^2 = 1 - c_1c_2\xi - c_2c_3\xi + c_1c_3\xi^2 \tag{21}$$

Substituting (18)−(21) into (5), the transfer function for the throughput port in Fig. 2**b** is given by

$$\frac{E_3(z)}{E_1(z)} = H_t^2 = \frac{c_1 - c_2\xi - c_1c_2c_3\xi + c_3\xi^2}{1 - c_1c_2\xi - c_2c_3\xi + c_1c_3\xi^2} \tag{22}$$

2.3.2. The transfer function $\frac{E_{12}(z)}{E_1(z)}$

There is only one forward path transmittance from node 1 to 12 for the drop port and since all loops touch this forward path, therefore

$$\begin{aligned} T_{1d}^2 &= js_1s_2s_3\xi \\ \Delta_1 &= 1 \end{aligned} \tag{23}$$

Substituting (21), (23) into (5), we get the transfer function for Fig. 2**b** at the drop port as

$$\frac{E_{12}(z)}{E_1(z)} = H_d^2 = \frac{js_1s_2s_3\xi}{1 - c_1c_2\xi - c_2c_3\xi + c_1c_3\xi^2} \tag{24}$$

2.4. Transfer functions of a triple ring resonator add/drop filter

SFG of a serially coupled triple ring resonator (STRR) filter is shown in Fig. 3**b**. Here the input node is $E_1(z)$ while $E_3(z)$ is considered as the throughput node and $E_{16}(z)$ is the drop node.

2.4.1. The transfer function $\frac{E_3(z)}{E_1(z)}$

There are six individual loop gains of the SFG being obtained and all the loop gains are expressed as

$$L_1^3 = c_1\sqrt{\xi}\, c_2\sqrt{\xi} = c_1c_2\xi \tag{25}$$

$$L_2^3 = c_2\sqrt{\xi}\, c_3\sqrt{\xi} = c_2c_3\xi \tag{26}$$

$$L_3^3 = c_3\sqrt{\xi}\, c_4\sqrt{\xi} = c_3c_4\xi \tag{27}$$

$$L_4^3 = c_1\sqrt{\xi}\,(-js_2)\sqrt{\xi}\, c_3\sqrt{\xi}\,(-js_2)\sqrt{\xi} = -c_1c_3s_2^2\xi^2 \tag{28}$$

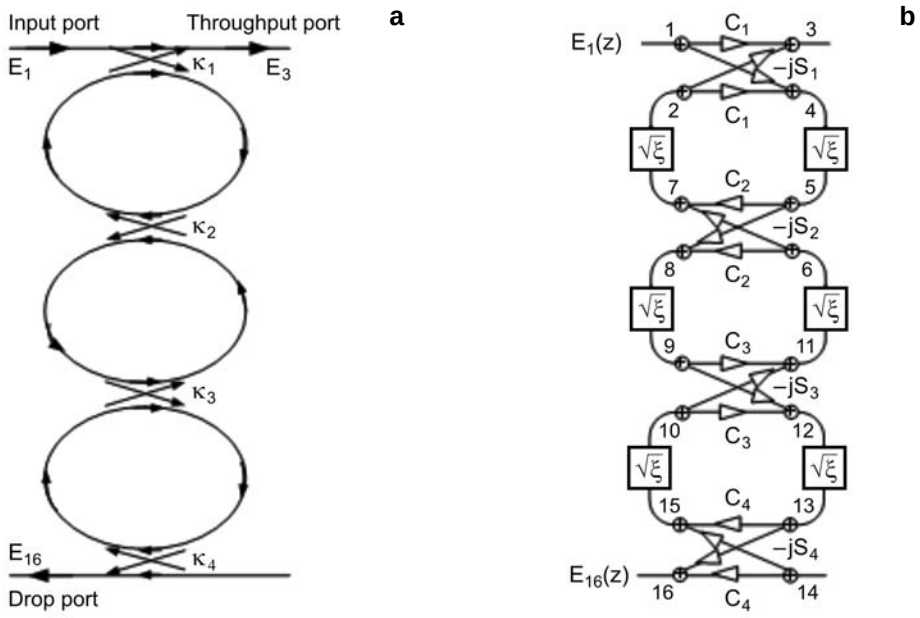

Fig. 3. The architecture of STRR add/drop filter: **a** – waveguide layout, **b** – Z-transform diagram (SFG).

$$L_5^3 = c_2\sqrt{\xi}\,(-js_3)\sqrt{\xi}\,c_4\sqrt{\xi}\,(-js_3)\sqrt{\xi} = -c_2c_4s_3^2\xi^2 \tag{29}$$

$$L_6^3 = c_1\sqrt{\xi}\,(-js_2)\sqrt{\xi}\,(-js_3)\sqrt{\xi}\,c_4\sqrt{\xi}\,(-js_3)\sqrt{\xi}\,(-js_2)\sqrt{\xi} = c_1c_4s_2^2s_3^2\xi^3 \tag{30}$$

There are five possible products of transmittance of two non-touching loops, given by:

$$L_{12}^3 = c_1c_2^2c_3\xi^2 \tag{31}$$

$$L_{23}^3 = c_2c_3^2c_4\xi^2 \tag{32}$$

$$L_{13}^3 = c_1c_2c_3c_4\xi^2 \tag{33}$$

$$L_{34}^3 = -c_1c_3^2c_4s_2^2\xi^3 \tag{34}$$

$$L_{15}^3 = -c_1c_2^2c_4s_3^2\xi^3 \tag{35}$$

There is one possible product of transmittance of three non-touching loops, given by

$$L_{123}^3 = c_1c_2^2c_3^2c_4\xi^3 \tag{36}$$

The forward path transmittances from node 1 to node 3 for the throughput port and its determinant which corresponds to the non-touching loop can be expressed as

$$\begin{aligned} T_{1t}^{3} &= (-js_1)\sqrt{\xi}\, c_2 \sqrt{\xi}\, (-js_1) = -c_2 s_1^2 \xi \\ \Delta_1 &= 1 - (L_2^2 + L_3^2 + L_5^2) + L_{23}^2 = \\ &= 1 - c_2 c_3 \xi - c_3 c_4 \xi + c_2 c_4 s_3^2 \xi^2 + c_2 c_3^2 c_4 \xi^2 \end{aligned} \tag{37}$$

$$\begin{aligned} T_{2t}^{3} &= (-js_1)\sqrt{\xi}\, (-js_2)\sqrt{\xi}\, c_3 \sqrt{\xi}\, (-js_2)\sqrt{\xi}\, (-js_1) = \\ &= c_3 s_1^2 s_2^2 \xi^2 \\ \Delta_2 &= 1 - L_3^3 = 1 - c_3 c_4 \xi \end{aligned} \tag{38}$$

$$\begin{aligned} T_{3t}^{3} &= (-js_1)\sqrt{\xi}\, (-js_2)\sqrt{\xi}\, (-js_3)\sqrt{\xi}\, c_4 \sqrt{\xi}\, (-js_3)\sqrt{\xi}\, (-js_2)\sqrt{\xi}\, (-js_1) = \\ &= -c_4 s_1^2 s_2^2 s_3^2 \xi^3 \\ \Delta_3 &= 1 \end{aligned} \tag{39}$$

$$\begin{aligned} T_{4t}^{3} &= c_1 \\ \Delta_4 &= 1 - (L_1^3 + L_2^3 + L_3^3 + L_4^3 + L_5^3 + L_6^3) + \\ &\quad + (L_{12}^3 + L_{23}^3 + L_{13}^3 + L_{34}^3 + L_{15}^3) - L_{123}^3 = \\ &= 1 - (c_1 c_2 \xi + c_2 c_3 \xi + c_3 c_4 \xi - c_1 c_3 s_2^2 \xi^2 - c_2 c_4 s_3^2 \xi^2 + c_1 c_4 s_2^2 s_3^2 \xi^3) + \\ &\quad + (c_1 c_2^2 c_3 \xi^2 + c_2 c_3^2 c_4 \xi^2 + c_1 c_2 c_3 c_4 \xi^2 - c_1 c_3^2 c_4 s_2^2 \xi^3 - c_1 c_2^2 c_4 s_3^2 \xi^3) + \\ &\quad - c_1 c_2^2 c_3^2 c_4 \xi^3 \end{aligned} \tag{40}$$

The loop determinant Δ of the SFG from (6) is the same with Δ_4 as (40) and by using the relation $s_i^2 + c_i^2 = 1$ (i = 2, 3), Δ simplifies to

$$\Delta = 1 - c_1 c_2 \xi - c_2 c_3 \xi - c_3 c_4 \xi + c_1 c_3 \xi^2 + c_2 c_4 \xi^2 - c_1 c_4 \xi^3 + c_1 c_2 c_3 c_4 \xi^2 \tag{41}$$

We can therefore obtain the transfer function for the throughput port as follow

$$\begin{aligned} \frac{E_3(z)}{E_1(z)} &= H_t^3 = \\ &= \frac{c_1 - c_2 \xi - c_1 c_2 c_3 \xi + c_3 \xi^2 - c_1 c_3 c_4 \xi + c_2 c_3 c_4 \xi^2 + c_1 c_2 c_4 \xi^2 - c_4 \xi^3}{1 - c_1 c_2 \xi - c_2 c_3 \xi - c_3 c_4 \xi + c_1 c_3 \xi^2 + c_2 c_4 \xi^2 - c_1 c_4 \xi^3 + c_1 c_2 c_3 c_4 \xi^2} \end{aligned} \tag{42}$$

2.4.2. The transfer function $\frac{E_{16}(z)}{E_1(z)}$

There is only one forward path transmittance from node 1 to 16 for the drop port and all loops also touch this forward path; therefore we have

$$T_{1d}^3 = (-js_1)\sqrt{\xi}\,(-js_2)\sqrt{\xi}\,(-js_3)\sqrt{\xi}\,(-js_4) = s_1 s_2 s_3 s_4 \xi^{3/2}$$
$$\Delta_1 = 1 \tag{43}$$

Substituting (41), (43) into (5), we obtain the transfer function in Fig. 3**b** at the drop port as

$$\frac{E_{16}(z)}{E_1(z)} = H_d^3 = \frac{s_1 s_2 s_3 s_4 \xi^{3/2}}{1 - c_1 c_2 \xi - c_2 c_3 \xi - c_3 c_4 \xi + c_1 c_3 \xi^2 + c_2 c_4 \xi^2 - c_1 c_4 \xi^3 + c_1 c_2 c_3 c_4 \xi^2} \tag{44}$$

3. Simulation results

The filtering responses of filters are simulated and discussed in this section. The filter characteristics as shown in Fig. 4 are the simulation results of the throughput and drop port of the SRR filter. The SRR has a radius equal to 136 μm, with the coupling coefficients of $\kappa_1 = \kappa_2 < 0.2$. The FSR of 100 GHz is achieved. The group refractive index is assumed to be $n_{gr} = 3.5$ and the internal loss is fully compensated ($\alpha = 0$). The on–off ratio is calculated and more than 20 dB obtained.

The maximum transmission characteristic of SRR as a function of κ_1 and κ_2 is shown in Fig. 5. The output intensities at the drop port will be unity at resonance ($\beta L = 2M_r\pi$), which indicates that the resonance wavelength is fully extracted by the resonator, for identical symmetrical couplers $\kappa_1 = \kappa_2$, especially lossless in waveguide ($\alpha = 0$) and couplers ($\gamma = 0$).

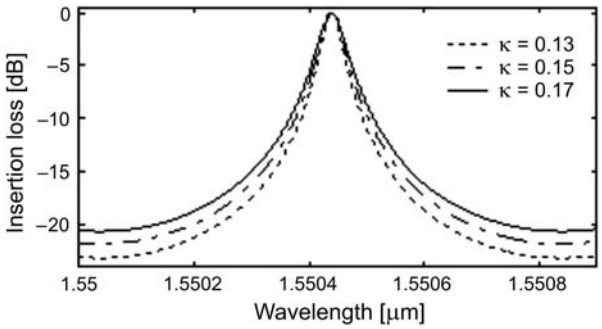

Fig. 4. The realization of high on–off ratio of the SRR, with $\kappa_1 = \kappa_2 = \kappa < 0.2$.

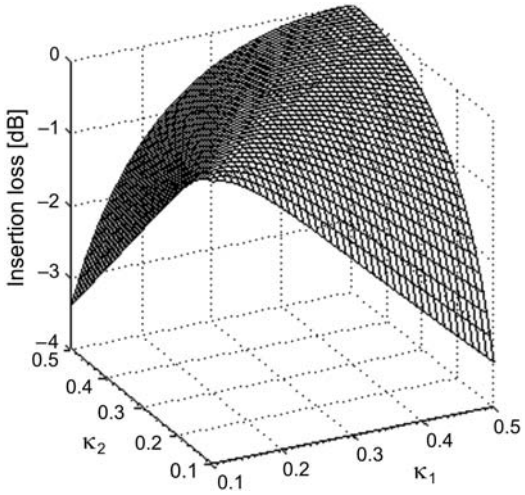

Fig. 5. The impact of κ_1 and κ_2 to transmittance characteristic at resonance for Fig. 1, when $\alpha = 0$ and $\gamma = 0$. Transmittance will be unity using symmetric coupling coefficient $\kappa_1 = \kappa_2$.

To design a box-like filter response shape, we increase the shape factor. It is reported that the improvement of the shape factor can be achieved by using multiple coupled ring resonators. In this paper, we restrict our investigation to the SDRR and STRR filters. Here, the SDRR and STRR filters radii are identically formed to SRR filter case, *i.e.*, R = 136 μm.

The simulated filter response of the SDRR is shown in Fig. 6. With full compensation of rings, a symmetric coupling coefficients is $\kappa_1 = \kappa_3 = 0.5$ for the outer couplers and $\kappa_2 = 0.12$ for the coupler at the center (solid line). The shape factor of the drop port for SDRR configuration is 0.41. The steep roll off and the flat top can be seen in the graph. In the graph of $\kappa_2 = 0.2$, 0.25 and 0.3, there are two points giving the peak response, which correspond to the two resonances. It means that every

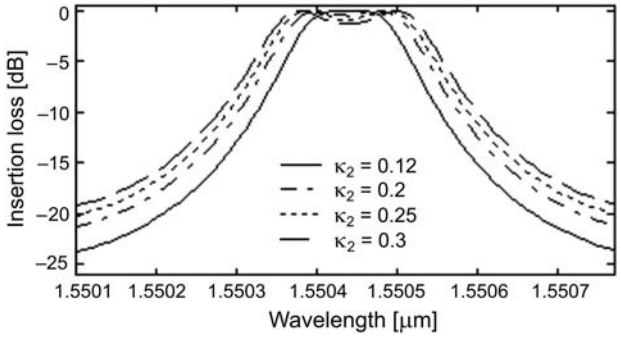

Fig. 6. Filter response of the drop port of the SDRR with coupling coefficients of $\kappa_1 = \kappa_3 = 0.5$, $\kappa_2 = 0.12$, 0.2, 0.25 and 0.3, $\alpha_{\text{ring1,2}} = 0$, $\gamma = 0$.

resonant point of a single ring is spliced into two when this is set coupled with another identical ring. One reason why the ripples are visible in the spectrum is the slight deviation from resonance mismatch of each involved SRR. Using the condition of maximum transmission on resonance ($\beta L = 2M_r\pi$) for the drop port, that is the Eq. (22) is set to be zero, and setting $\kappa_1 = \kappa_3$, $\alpha_{\text{ring1,2}} = 0$, $\gamma = 0$, the value for the coupler in the center κ_2 is

$$\kappa_{2c} = \frac{\kappa_1^2}{(\kappa_1 - 2)^2} \tag{45}$$

where we define κ_{2c} as the critical coupling coefficient. We have found that if κ_2 is decreased reaching κ_{2c}, the two resonances as Fig. 7 will merge back into the resonance point. Figure 7 shows the case of $\kappa_2 < \kappa_{2c}$, which results the decreasing in output amplitude become excess loss although the waveguide does not have any propagation loss. It is clarified that $\kappa_2 = \kappa_{2c}$ is the optimum coupling ratio for minimizing excess loss at the resonance point. Besides, for realizing a box-like filter shape for lossless SDRR, the on–off ratio of the drop port of greater than 20 dB is also achieved using

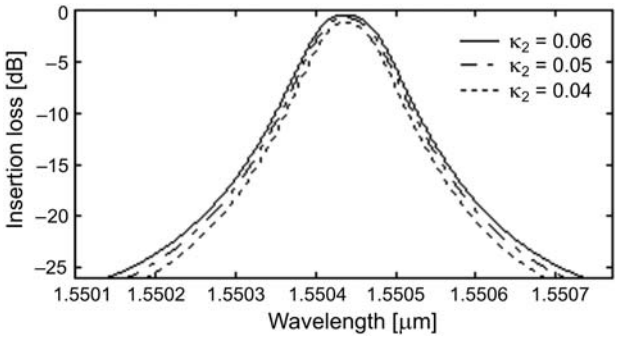

Fig. 7. The transmittance value of the SDRR comparing to the different values of κ_2 is lower than κ_{2c} and $\kappa_1 = \kappa_3 = 0.5$, $\alpha_{\text{ring1,2}} = 0$, $\gamma = 0$.

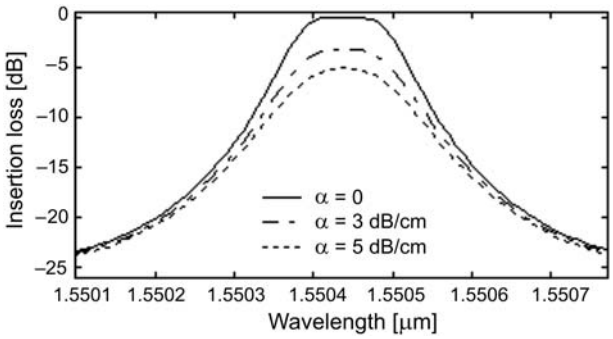

Fig. 8. The impact of attenuation coefficient to box-like filter shape and amplitude of the drop port of the SDRR with $\kappa_1 = \kappa_3 = 0.5$, $\kappa_2 = 0.13$.

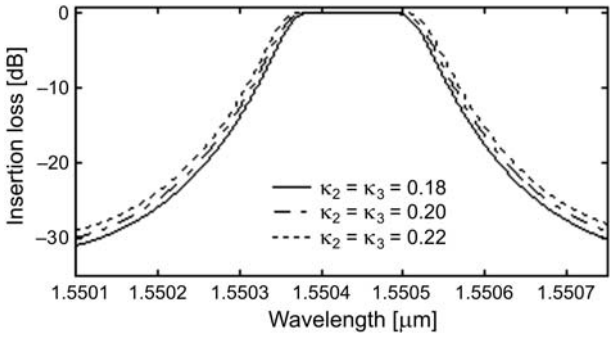

Fig. 9. The realization of box-like filter shape of the STRR with coupling coefficients $\kappa_{1,4} = 0.65$, $\kappa_{2,3} = 0.18-0.22$, with lossless $R = 136$ μm.

the same coupling coefficients for the outer couplers, and κ_2 is within the narrow range 0.12–0.14. The influence of optical loss of the SDRR with α equal to 3 and 5 dB/cm is shown in Fig. 8. We notice that optical loss in ring resonators will result in decreasing in the shape factor and output amplitude.

Figure 9 illustrates the simulated filter response of the STRR which is used to achieve shape factor. For simplification, we set $\kappa_1 = \kappa_4$ and $\kappa_2 = \kappa_3$, and the filter response for the drop port with coupling coefficients of $\kappa_1 = \kappa_4 = 0.65$ for the outer couplers and $\kappa_2 = \kappa_3 = 0.18-0.22$ for the center couplers with $\alpha_{\text{ring1,2,3}} = 0$, $\gamma = 0$, are used. The on–off ratio is approximately 30 dB is noted while the shape factor of the drop port is up to 0.6.

A flatter top, steeper roll-off and higher out-of band rejection are achieved with this configuration. A possible solution to achieve a box-like filter shape with the shape factor of approximately 0.6 and an on–off ratio of more than 30 dB is obtained for lossless resonators and couplers, and they also use for coupling coefficients within the range of $\kappa_1 = \kappa_4 = 0.65-0.67$, and $\kappa_2 = \kappa_3 = 0.18-0.22$ for the outer and center couplers, respectively. Another possibility of achieving a box-like filter is to use coupling coefficients of $\kappa_1 = \kappa_4 = 0.5$ and $\kappa_2 = \kappa_3 = 0.08-0.1$. This configuration

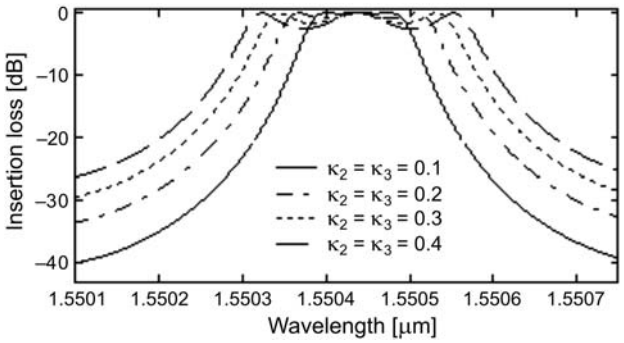

Fig. 10. Filter response of the drop port of the STRR with coupling coefficients of $\kappa_{1,4} = 0.5$, $\kappa_{2,3} =$ $= 0.1-0.4$, and $\alpha_{\text{ring1,2}} = 0$, $\gamma = 0$.

T a b l e. Characteristics data comparison between SRR and SMRR filters.

Filter order	Single	Double	Triple
Shape factor	0.16	0.42	0.6
Cross talk	–20 dB	> –20 dB	> –30 dB
Box-like shape	No	Yes	Yes

enables an on–off ratio of more than 30 dB and a shape factor of 0.6, as an example of $\kappa_{1,4} = 0.5$, $\kappa_{2,3} = 0.1$ (solid line), as shown in Fig. 10. Similarly, for the values of $\kappa_2 = 0.2-0.4$, there are three points giving the peak response due to the slight deviation from resonance mismatch of each involved single ring resonator. The simulation results of some filter response parameters such as the shape factor, cross talk, and box-like shape of the lossless SRR, DRR, and TRR filters are compared as shown in the Table.

4. Vernier effect

Serially coupled multiple ring resonator filters open the possibility of expanding the FSR to the least common multiple of the FSR of individual ring resonators. This is done by choosing different radii in the SMRR, which is called the Vernier operation. In the case of different radii, the light passing through the SMRR is launched from the drop port when the resonant conditions of the multiple single ring resonators are satisfied. We investigated two and three rings serially coupled Vernier filters.

Referring to Fig. 11**a**, which is shown the SDRR Vernier filter architecture, where the SFG is shown in Fig. 11**b**. Vernier operation of SDRR with two different radii is expressed by:

$$\mathrm{FSR} = N\,\mathrm{FSR}_1 = M\,\mathrm{FSR}_2 \tag{46}$$

which leads to:

$$\mathrm{FSR} = |M - N|\,\frac{\mathrm{FSR}_1\,\mathrm{FSR}_2}{|\mathrm{FSR}_1 - \mathrm{FSR}_2|} \tag{47}$$

where N and M are natural and co-prime numbers and have to be carefully designed to make sure that both N and M are integers ($M > N$). To determine the transfer function of SDRR Vernier filter, which is similar to the transfer functions as shown in Sections 2.2 and 2.3, but the different setting in parameters of x- and z-transforms is employed. The transfer function of SFG in Fig. 11**b** for the drop port is therefore expressed by

$$\frac{E_{12}(z)}{E_1(z)} = H_d^2 = \frac{j s_1 s_2 s_3 \sqrt{x_1 x_2}\,\sqrt{z^{-(N+M)}}}{1 - c_1 c_2 x_1 z^{-N} - c_2 c_3 x_2 z^{-M} + c_1 c_3 x_1 x_2 z^{-(N+M)}} \tag{48}$$

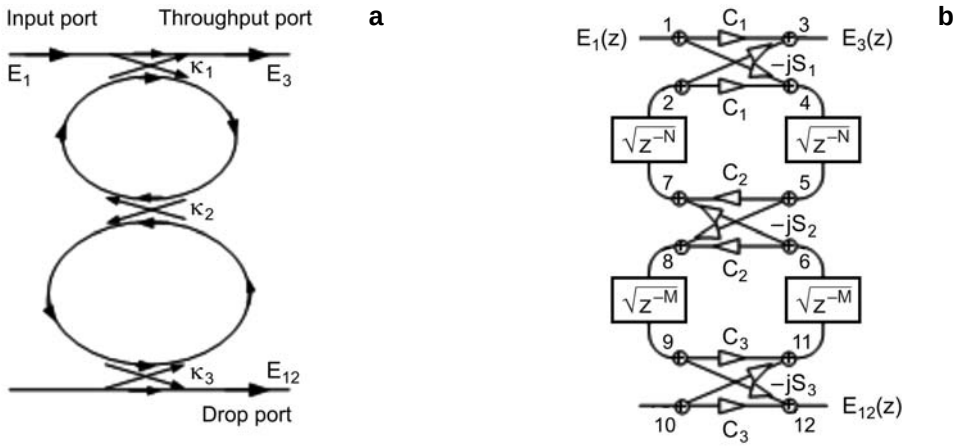

Fig. 11. The architecture of SDRR Vernier filter: **a** – waveguide layout, **b** – *Z*-transform diagram (SFG).

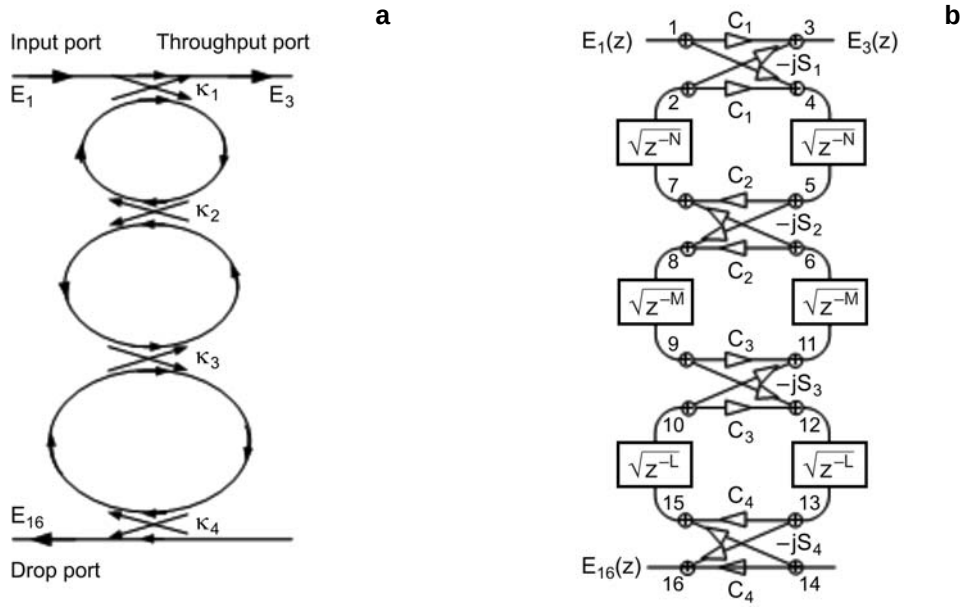

Fig. 12. The architecture of STRR Vernier filter: **a** – waveguide layout, **b** – *Z*-transform diagram (SFG).

where $x_i = \exp(-\alpha L_i/2)$ $(i = 1, 2)$ are the ring losses of the ring 1 and ring 2, respectively.

The architecture of STRR Vernier filter is shown in Fig. 12**a** and Fig. 12**b** shows its SFG. FSR of STRR with three different radii is expressed by:

$$\mathrm{FSR} = N\,\mathrm{FSR}_1 = M\,\mathrm{FSR}_2 = L\,\mathrm{FSR}_3 \tag{49}$$

where N, M and L are resonant numbers for each ring resonator and all are integers ($L > M > N$). Similarly, the transfer function of SFG in Fig. 12**b** for the drop port is expressed by

$$\frac{E_{16}(z)}{E_1(z)} = H_d^3 = \frac{s_1 s_2 s_3 s_4 \sqrt{x_1 x_2 x_3}\ \sqrt{z^{-(N+M+L)}}}{A} \tag{50}$$

where

$$A = 1 - c_1 c_2 x_1 z^{-N} - c_2 c_3 x_2 z^{-M} - c_3 c_4 x_3 z^{-L} + c_1 c_3 x_1 x_2 z^{-(N+M)} + \\ + c_2 c_4 x_2 x_3 z^{-(M+L)} + c_1 c_2 c_3 c_4 x_1 x_3 z^{-(N+L)} - c_1 c_4 x_1 x_2 x_3 z^{-(N+M+L)}$$

while $x_i = \exp(-\alpha L_i/2)$ (i = 1, 2, 3) are the ring losses of the ring 1, 2 and 3 from top to bottom. Normally, the couplers adjacent to the bus waveguides (κ_1 and κ_N) are stronger than the innermost couplers.

First, we present the Vernier effect of SDRR filter followed by the corresponding result on STRR filter. In this study, we choose the SDRR Vernier filter with R_1 = 273 μm, R_2 = 341 μm and use symmetric coupling coefficients of $\kappa_{1,3}$ = 0.5 for the outer couplers and κ_2 = 0.13 for the coupler at the center with lossless in waveguides (α = 0) and couplers (γ = 0). According to Eq. (2), the FSR for each single ring resonator of resonator 1 is 50 GHz and FSR of resonator 2 is 40 GHz and FSR of SDRR is calculated to be 200 GHz as shown in Fig. 13. Therefore, the resonant

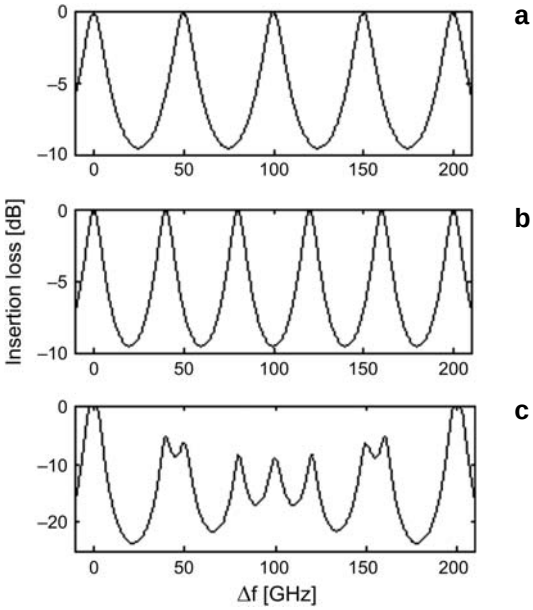

Fig. 13. Optical frequency response of SDRR Vernier filter of each ring resonator: resonator 1 with FSR_1 = 50 GHz (**a**), resonator 2 with FSR_2 = 40 GHz (**b**), and of the DRR with FSR = 200 GHz (**c**).

numbers for each ring resonator are designed to be $N = 4$, $M = 5$. The interstitial resonances suppression of the drop port is approximately 5.2 dB.

The suppression of interstitial resonances of the SDRR is as shown in Fig. 14. This can be improved by decreasing the coupling coefficient of the center coupler to be $\kappa_2 = 0.08, 0.05$, where the other parameters are set identical to Fig. 13. The interstitial resonances suppression of 6.9 dB (solid line) and 8.8 dB (dash line) are respectively achieved. We have found that the decrease of κ in the coupler center effects a little the deterioration of resonant loss at resonance peaks. By setting the coupling coefficients of $\kappa_1 = \kappa_3 = 0.5$ for the outer couplers and within the tolerances of $\kappa_2 = 0.09-0.13$ for the coupler in the center, a possible solution for achieving the side mode suppression of more than 5 dB with lossless at resonance peaks can be obtained.

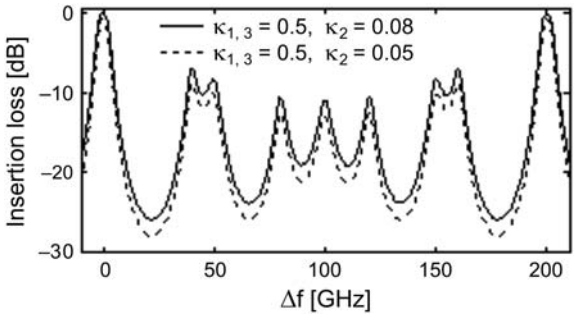

Fig. 14. The improvement in suppression of interstitial resonances of SDRR Vernier filter.

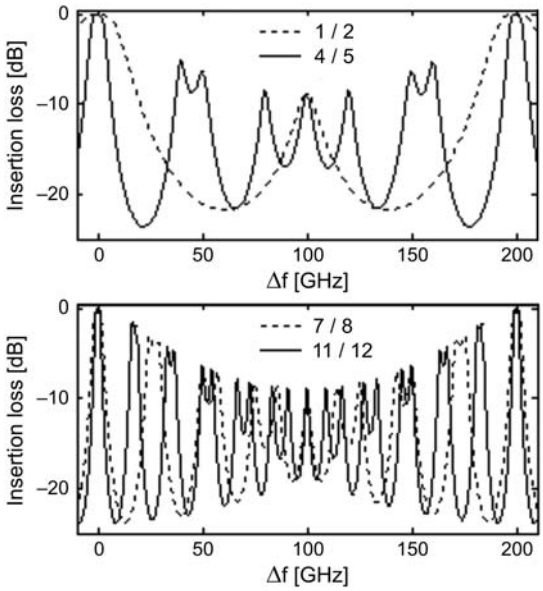

Fig. 15. Comparison of SDRR Vernier filter response with different FSR ratios $N:M$ = 1:2, 4:5, 7:8, and 11:12.

Figure 15 shows a comparison of the calculated magnitude responses for FSR ratios N:M of 1:2, 4:5, 7:8, and 11:12 and other parameters. These ratios are given the same FSR which is equal to 200 GHz. Note the increasing interstitial resonances for the ratios of larger integer values. The passband width of the resonant transmission peak is dominated by the largest ring; consequently, the response can be made sharper only at the expense of reducing the passband width. For this reason, the best FSR of DRR Vernier in Fig. 15 is a resonance number 4:5 which is suitable to design the FSR expansion. Similar result can also be obtained when using a resonance number 1:2, however, in this case it affects the device bending loss due to the decreasing ring radius.

The SDRR Vernier effect filter does not offer sufficient suppression of the interstitial resonances, while those that consist of more than four rings are too complex and expensive to fabricate, and moreover they fail to provide needed improvement in suppression. In order to improve the suppression of interstitial resonances, three- and four-ring series coupled Vernier effects will be used. In this study, the next simulation of filter was mainly focused on the STRR Vernier effect. Another advantage of STRR Vernier filter can be designed to reduce the unit delay length as half of the SDRR Vernier filter, where the double FSR in comparison with SDRR Vernier filter can be achieved.

The frequency responses of the STRR Vernier filter with R_1 = 273 μm, R_2 = = 341 μm and R_3 = 511 μm by using symmetric coupling coefficients of $\kappa_{1,4}$ = 0.5 and $\kappa_{2,3}$ = 0.01 are shown in Fig. 16. The FSR of resonator 1 is 50 GHz, the FSR of resonator 2 is 40 GHz and the FSR of resonator 3 is 26.67 GHz from top to bottom

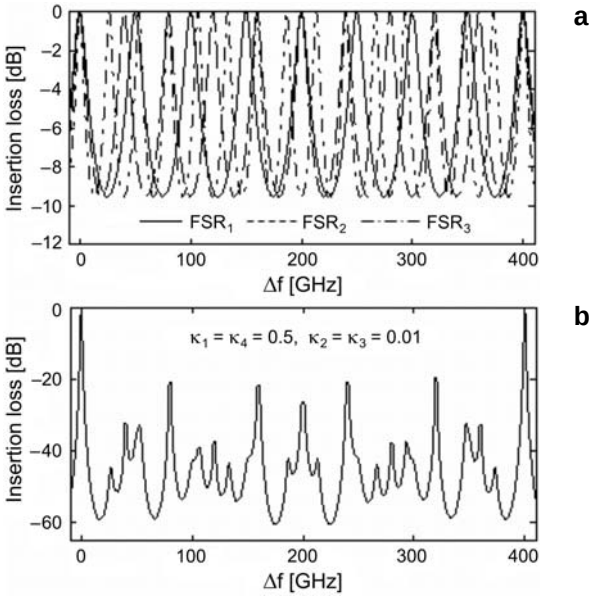

Fig. 16. Frequency response of STRR Vernier filter of each ring resonator: (**a**) FSR_1 = 50 GHz, FSR_2 = 40 GHz, FSR_3 = 26.67 GHz and (**b**) of the TRR with FSR = 400 GHz.

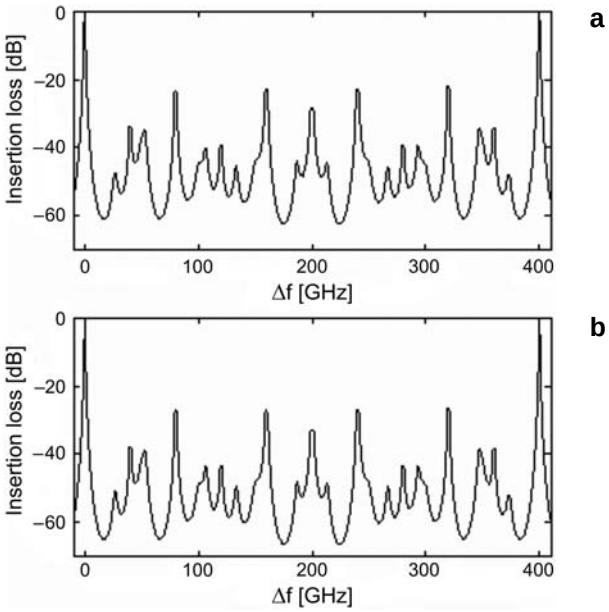

Fig. 17. The improvement in suppression of interstitial resonances of STRR Vernier filter: $\kappa_{1,4} = 0.5$, $\kappa_{2,3} = 0.008$ (**a**), $\kappa_{1,4} = 0.5$, $\kappa_{2,3} = 0.005$ (**b**).

as shown in Fig. 16**a**. The FSR of the STRR Vernier is calculated using Eq. (2) to be 400 GHz as shown in Fig. 16**b**, which achieves the double FSR in comparison with SDRR Vernier. Here, the resonant numbers for each ring resonator are designed to be $N = 8$, $M = 10$ and $L = 15$. The interstitial resonances suppression of the drop port is noted to be 18.5 dB. In order to suppress the interstitial resonances, the lower coupling coefficients in the center couplers having the advantage are shown in Fig. 17. Here, the parameters of STRR Vernier filter are identical as in Fig. 16. The interstitial resonances suppression for the drop port with $\kappa_1 = \kappa_4 = 0.5$, $\kappa_2 = \kappa_3 = 0.008$ is approximately 22 dB, and $\kappa_1 = \kappa_4 = 0.5$, $\kappa_2 = \kappa_3 = 0.005$ is 26.5 dB as shown in Figs. 17**a** and 17**b**, respectively. However, we have found that the response of STRR Vernier filter will be reduced in the passband width, while it is sharper at the resonance peaks.

5. Conclusions

We have proposed a novel attempt to employ a graphical approach in the analytical derivation of the optical transfer functions of SMRR filters. The graphical approach with SFG is used in our analysis for fast derivation of the optical transfer functions. The improvement of a box-like passband shape using the serially coupled multiple ring resonators has been presented. The shape factor of SDRR and STRR with loss compensation has successfully increased to 0.42 and 0.6, respectively, which is more than 0.16 of the SRR filter. A flatter top, steeper roll-off and a higher out of band

rejection > 20 dB has been achieved both for SDRR and STRR filter. The influence of the optical loss in ring resonators of SDRR and STRR has also been analyzed and it has been found that it had an effect on the deterioration of a box-like shape in passbands and resonant peaks. In addition, the SMRR filters have been investigated which exploit the Vernier effect. This opens the possibility to realize a larger FSR than would be achieved using only a single ring resonator. The suppression of interstitial resonances of the SDRR Vernier has been improved by decreasing the coupling coefficient of the center coupler. We have noted the increasing interstitial resonances for the ratios of larger integer values. Note that the SDRR Vernier filter does not adequately suppress the interstitial resonances that lie between the main resonances separated by the FSR. A solution to this problem can be presented using STRR Vernier filter. In addition, the advantage of STRR Vernier filter can be designed to obtain double FSR in comparison with DRR Vernier filter.

References

[1] MELLONI A., MARTINELLI M., *Synthesis of direct coupled-resonators bandpass filters for WDM systems*, IEEE Journal of Lightwave Technology **20**(2), 2002, pp. 296–303.

[2] LITTLE B.E., CHU S.T., HAUS H.A., FORESI J.S., LAINE J.-P., *Microring resonator channel dropping filters*, IEEE Journal of Lightwave Technology **15**(6), 1997, pp. 998–1005.

[3] HRYNIEWICZ J.V., ABSIL P.P., LITTLE B.E., WILSON R.A., HO P.T., *Higher order filter response in coupled microring resonators*, IEEE Photonics Technology Letters **12**(3), 2000, pp. 320–322.

[4] LITTLE B.E., CHU S.T., PAN W., RIPIN D., KANEKO T., KOKUBUN Y., IPPEN E., *Vertically coupled glass microring resonator channel dropping filters*, IEEE Photonics Technology Letters **11**(2), 1999, pp. 215–217.

[5] SUZUKI S., ODA K., HIBINO Y., *Integrated-optic double-ring resonators with a wide free spectral range of 100 GHz*, IEEE Journal of Lightwave Technology **13**(8), 1995, pp. 1766–1771.

[6] SOREL M., GLUCK S., LAYBOURN P.J.R., *Semiconductor double ring waveguide resonator*, Electronics Letters **35**(18), 1999, pp. 1551–1552.

[7] YANAGASE Y., SUZUKI S., KOKUBUN Y., SAI TAK CHU, *Box-like filter response and expansion of FSR by a vertically triple coupled microring resonator filter*, IEEE Journal of Lightwave Technology **20**(8), 2002, pp. 1525–1529.

[8] MADSEN C.K., ZHAO J.H., *Optical Filter Design and Analysis: A Signal Processing Approach*, Wiley, New York 1999.

[9] SCHWELB O., *Generalized analysis for a class of linear interferometric networks. I. Analysis*, IEEE Transactions on Microwave Theory and Techniques **46**(10), 1998, pp. 1399–1408.

[10] CAPMANY J., MURIEL M.A., *A new transfer matrix for the analysis of fiber ring resonators: compound coupled structures for FDMA demultiplexing*, IEEE Journal of Lightwave Technology **8**(12), 1990, pp. 1904–1919.

[11] MOSLEHI B., GOODMAN J.W., TUR M., SHAW H.J., *Fiber-optic lattice signal processing*, Proceedings of the IEEE **72**(7), 1984, pp. 909–930.

[12] MASON S.J., *Feedback theory-further properties of signal flow graphs*, Proceedings of the IRE **44**(7), 1956, pp. 920–926.

Received May 13, 2008